

**Figure 9** Measured results of radiation patterns:(a)  $H$ -plane, (b)  $E1$ -plane, and (c)  $E2$ -plane are for 0.9-GHz antenna; (d)  $H$ -plane, (e)  $E1$ -plane, and (f)  $E2$ -plane are for 1.8-GHz antenna

to radiation patterns obtained from numerical simulation, wherein neither coaxial cable nor unbalanced current is introduced in the simulation process. Measurements of 3D far-field radiation patterns of antennas are performed in an anechoic chamber with a length of 10 m, width of 7 m, and height of 7 m.

#### 4. CONCLUSION

A design method using equivalent  $L$ - $C$  circuit for coaxial transmission-line discontinuity was presented to implement a dual-band balun with stacked coaxial cavities. The method expedited the design process of the dual-band balun that requires large computer simulation and optimization process for the dimensions. In particular, a wide range of ratio of the upper resonant frequency to the lower resonant frequency was obtained by changing the radii of the stacked cavities. Experimental results revealed that the presence of the balun improved the measurement accuracy of the radiation patterns of printed monopole antennas.

#### ACKNOWLEDGMENTS

This work was supported by the National Science Council, R.O.C., under Grant NSC95-2221-E-011-022-MY2.

#### REFERENCES

1. C. Ichelin, J. Krogerus, and P. Vainikainen, Use of balun chokes in small-antenna radiation measurements, *IEEE Trans Instrum Meas* 53 (2004), 498-506.
2. Y.L. Chow, K.F. Tsang, and C.N. Wang, An accurate method to measure the antenna impedance of a portable radio, *Microwave Opt Technol Lett* 23 (1999), 349-352.
3. T. Taga, Analysis for mean effective gain of mobile antennas in land mobile radio environments, *IEEE Trans Veh Technol* 39 (1990), 117-131.
4. O. Staub, J.-F. Zurcher, and A. Skrivervik, Some considerations on the correct measurement of the gain and bandwidth of electrically small antennas, *Microwave Opt Technol Lett* 17 (1998), 156-160.
5. Z.-Y. Zhang, Y.-X. Guo, L.C. Ong, and M.Y.W. Chia, A wide-band planar balun on a single-layer PCB, *IEEE Microwave Wireless Compon Lett* 15 (2005), 416-418.
6. K.S. Ang and I.D. Robertson, Analysis and design of impedance-transforming planar Marchand balun, *IEEE Trans Microwave Theory Tech* 49 (2001), 4402-4406.
7. J.R. Whinnery, H.W. Jamieson, and T.E. Robbins, Coaxial-line discontinuities, *Proc IRE* 32 (1944), 1944, 695-709.

© 2008 Wiley Periodicals, Inc.

## NEURAL NETWORK ESTIMATION OF RF ELECTROMAGNETIC POLLUTION NEAR TV BROADCAST TRANSMITTERS

İlhami Çolak<sup>1</sup> and İlhan Koçsalay<sup>2</sup>

<sup>1</sup> Department of Electrical Education, Faculty of Technical Education, Gazi University, 06500 Besevler, Ankara, Turkey; Corresponding author: icolak@gazi.edu.tr

<sup>2</sup> Turkish Radio and Television (TRT) Authorization, Studio Planning Department, Oran, Ankara, Turkey

Received 21 August 2007

**ABSTRACT:** A set of measurements to investigate the Radio Frequency (RF) electromagnetic pollution in an area surrounding a TV broadcast transmitter has been given. The RF electromagnetic fields at different transmitter output power and time, in and out of the measurement points, were estimated and visualized by the developed visual software, which has 3D screening unit, based on Artificial Neural Network and Grid Data. The software enables users to estimate the RF electromagnetic field distributions in and out of the measurement points. Electric and magnetic field components of RF radiation value at any point/area can be compared with national/international standard limits easily using the software developed. © 2008 Wiley Periodicals, Inc. *Microwave Opt Technol Lett* 50: 1004–1010, 2008; Published online in Wiley InterScience (www.interscience.wiley.com). DOI 10.1002/mop.23301

**Key words:** TV transmitter; RF radiation measurements; artificial neural networks; estimation

#### 1. INTRODUCTION

Radiation produced by radio frequency electromagnetic field source propagate far distances. RF fields are generated by, among others, mobile (tele) phones and base stations, television and radio transmitters, and radar systems.

RF radiation from broadcasting transmitters has led to put certain regulations and control in some countries. There are lots of international or national standards which recommend measurement method and levels of electromagnetic field for safety purpose [1–4].

In addition to official TV broadcasting, there was a tremendous increase in the number of private TV and radio stations all over the

world during the last decade. So, number of transmitter antennas has been increased as well.

TV transmitter antennas radiate electromagnetic waves up to 2 MW which is extremely high. Most of the transmitter antennas are located in city center and cause an increase in radiation hazard on human health. Inside transmitter station and close to the transmitter antenna, electric and magnetic field can sometimes exceed the safety standards. RF radiation hazards could also reach the limits of the safety standards outside the broadcasting station [5, 6]. Although people are focusing on the GSM transmitter and antennas, live data of measured values and some simulations show that TV transmitter produce higher electromagnetic wave than GSM transmitters [7]. Because of its lower frequency, at similar RF exposure levels, the body absorbs up to five times more of the signal from TV transmitter than from GSM transmitters (base stations). This is because the frequencies used in TV broadcasting (around 300–400 MHz) are lower than those employed in mobile telephony (900 MHz and 1800 MHz). So, it is very important to measure and estimate RF radiation near TV transmitter and buildings.

Kahski and Stasiński [8] presented an approximate numerical technique for estimation of the near EM field distribution in the vicinity of broadcast FM and TV antenna systems. Method was based on some assumptions and complex theory.

Al-Ruwais [5] studied far field measurements of electric and magnetic fields in an area surrounding the MW and SW broadcast stations in Ryadh, Saudi Arabia and estimated values of the electric fields contribution from each of the MW and SW stations separately. They are then discussed and compared with the most up to date radiation safety standards.

Faraone et al. [9] investigated the character of the average power density in the close proximity of base-station antennas.

Shay et al. [10] proposed new measurement method for radiation from AM, FM, TV, and mobile phone base stations. They said that the measurement points could be chosen with equal spacing on the three lines within the 3 dB beam width for both horizontal and vertical polarization.

Cicchetti and Faraone [11] suggested prediction formulae for estimating the peak equivalent power density in the near-field of cellular base-station array antennas. The prediction formulae had a built-in conservative bias to yield an overestimation of the actual exposure levels, which is desirable for compensating perturbations due to the environment.

Larcheveque et al. [12] studied the impact of small-scale fading on the estimation of local average power density for radio frequency exposure assessment.

Joseph et al. [13] presented a low-cost measurement method for the extraction of the relative phases of the field of base station and broadcast antennas. They claimed, using the method and knowing the polarization of the incident field, it is able to be determined more accurately the actual electromagnetic power absorbed in people at a measurement site.

All these studies have been recently worked on. RF EMFs have been visualized in two dimensions at the measurement points in many cases. And complex analytical methods were used at most of them. Until now, RF EMFs estimation study based on measured data has not been mentioned in literature.

In this study, RF EMFs have been represented in 3D covering all points around a transmitter center. Visual software, which has 3D screening unit, based on ANNs has been developed. This provides that researchers might consider the effects of distributions around electrical and biological environments more clearly, effectively, and efficiently. In addition, the software developed enables

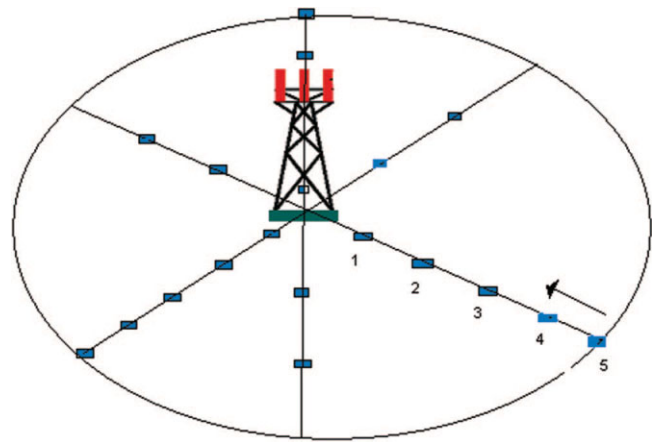


**Figure 1** Measurement points near the antenna. [Color figure can be viewed in the online issue, which is available at [www.interscience.wiley.com](http://www.interscience.wiley.com)]

users to compare electrical and magnetic fields measured-estimated at any point with national or international standards.

## 2. MEASUREMENTS AND INVESTIGATIONS

RF EMFs around Turkish Radio and Television Authority (TRT) TV transmitter antenna (Ankara-Dikmen/TURKEY) were measured by EMR-300 radiation meter. Measurement points are shown at Figure 1. Measurements of EMFs were achieved at 1.75 m above ground for 1000 W output power. Many contemporary guidelines and standards, including IEEE Std C95.1-1991, specify the maximum permissible values of the RF field strength or power density as averaged over a specified averaging time, e.g., any continuous 6 min or 30 min interval. The time-averaging provision permits exposures that exceed the maximum permissible exposure (MPEs) for continuous exposure when the exposure duration is less than the averaging time. EMR-300 was held 6 min for every measurement. Measured values indicated in the Table 1 are total electric and magnetic fields for remarked point. Figure 2 shows a photograph of the measured area. Free-space electromagnetic fields of measured area are not due to a single source, measured fields values are the result of several transmitters from different directions. To be able to correctly determine the radiation exposure, any measurement must be nondirectional. The value measured by an isotropic instrument is also not affected by the position in which the instrument is used. The probes of EMR-300 were fitted with three sensors which measure the field strength of the X-, Y-, and Z-directions separately. The field strength is calculated by the instrument's processor by summing the squares of the three measured values.

Measurements in Table 1 were taken when transmitter output power was 1000 W and 09:00 am and 13:00 pm time period and given as an example measurements. Furthermore, six sets of measurements were made for ANN training and comparing. Other measurement periods are 05:00 am and 09:00 am, 13:00 pm and 18:00 pm, 18:00 pm, and 24:00 pm. Essentially, all measurements were made within 19 windows between 05:00 am and 24:00 pm. Every measurement was done without fluctuation in the transmitter output power.

ANN based developed program, written in C++ users, can estimate distribution of EMF not only at the defined points but also at every point around the transmitter. The benefits of accurately predicting EMF distribution around antennas are proper design of antennas with radiation issue in mind, risk estimation of exposure

**TABLE 1 Measurement Values Near the TRT TV Transmitter (Ankara-Dikmen/Turkey)**

Antenna (sektor)	Distance From Antenna (m)	Measured Magnetic Field (A/m)	Measured Electric Field (V/m)	Measured Time	Type of Antenna	Remarkd Measure Point
1	10	0.025	7.06	10:30	Pano	1
1	15	0.026	7.57	10:40	Pano	2
1	25	0.027	9.06	10:50	Pano	3
1	45	0.035	13.20	11:50	Pano	4
1	60	0.058	26.33	12:00	Pano	5
2	10	0.023	9.50	11:00	Pano	1
2	15	0.038	8.00	11:10	Pano	2
2	20	0.027	7.56	11:15	Pano	3
2	45	0.029	11.35	12:10	Pano	4
2	60	0.050	21.04	12:20	Pano	5
3	10	0.023	8.06	11:25	Pano	1
3	15	0.024	8.06	11:35	Pano	2
3	20	0.025	7.58	11:45	Pano	3
3	45	0.049	19.01	12:30	Pano	4
3	60	0.072	28.02	12:40	Pano	5
1-2	20	0.019	6.02	09:20		
1-2	40	0.044	17.53	09:30		
1-2	60	0.063	24.55	09:40		
2-3	20	0.026	7.30	09:50		
2-3	40	0.030	12.05	10:00		
3-1	20	0.025	7.40	10:10		
3-1	40	0.036	14.20	10:20		

to EMF, better understanding of electric and magnetic properties of biological tissues.

**3. ARTIFICIAL NEURAL NETWORKS**

Multilayered perceptrons (MLPs), which are among simplest and therefore most commonly used ANN structures (see Fig. 3), have been adapted for many applications [14–17]. Inputs to the network are passed to each neuron in input layer. Outputs of neurons in the first layer become inputs to the hidden layer and so on. Neurons in the input layer only act as buffers for distributing input signals  $x_i$  to neurons in the hidden layer. Each neuron  $j$  in hidden layer sums up its input signals  $x_i$  after weighting them with strengths of respective weight connections  $w_{ji}$  from the input layer and computes its output  $y_j$ , which is the output of  $j$ th neuron in the hidden or output layer, as a function  $f$  of the sum,

$$y_j = f(\text{net}_j), \tag{1}$$

with

$$\text{net}_j = \sum_i w_{ji} x_i + \theta_j \tag{2}$$

where  $f$  is a transfer or activation function and can be a sigmoid or a hyperbolic tangent function, and  $\theta_j$  is a variable bias with similar function to a threshold. The transfer function has the feature of being nondecreasing and differentiable. Note that  $y_j$  can be defined recursively in terms of its inputs. The computation continues until output of the network is found. After computing the output, the training process starts in according with the learning algorithm used.

Back propagation with momentum (BPM) learning algorithm, a gradient descent algorithm, has been selected for training in this



**Figure 2** TRT TV transmitter antenna and Private TV, Radio transmitter antennas near the TRT TV transmitter antenna. [Color figure can be viewed in the online issue, which is available at [www.interscience.wiley.com](http://www.interscience.wiley.com)]

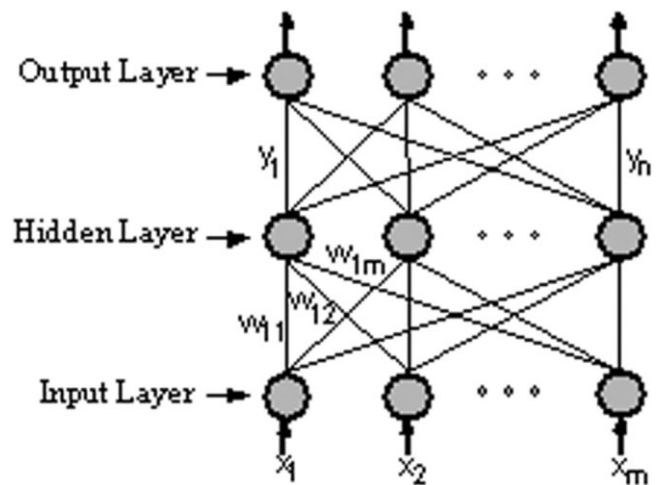


**Figure 3** Topology of multilayered perceptron

work. Basically, learning in an MLP is to find a set of weights that minimizes mismatching between network outputs and target values. It is an iterative training process in which an output error is propagated back through the layers and used to modify weights. The error  $E$  is defined by

$$E = \sum_p E_p = \frac{1}{2} \sum_p \sum_i (ty_{pj} - y_{pj})^2 \quad (3)$$

where  $ty_j$  is the desired or target value of output for a given input, and the summation is performed over all output neurons  $j$ . Once the outputs from hidden layers and output layer have been calculated for each input pattern  $p$ , direction of steepest descent in parameter space is determined by the following partial derivatives of  $E$

$$-\frac{\partial E}{\partial w_{ji}} = \sum_p \delta_{pj} y_{pi} \quad (4)$$

$$-\frac{\partial E}{\partial \theta_j} = \sum_p \delta_{pj} \quad (5)$$

where  $\delta_{pj}$  can be calculated as

$$\delta_{pj} = -\frac{\partial E_p}{\partial \text{net}_{pj}} = -\frac{\partial E_p}{\partial y_{pj}} \frac{\partial y_{pj}}{\partial \text{net}_{pj}} \quad (6)$$

with

$$\frac{\partial y_{pj}}{\partial \text{net}_{pj}} = (1 - y_{pj})(1 + y_{pj}) \quad (7)$$

$$\frac{\partial E_p}{\partial y_{pj}} = \frac{\partial}{\partial y_{pj}} \sum_j \frac{1}{2} (ty_{pj} - y_{pj})^2 = -(ty_{pj} - y_{pj}) \quad (8)$$

$$\frac{\partial E_p}{\partial y_{pj}} = \sum_k \frac{\partial E_p}{\partial \text{net}_{pk}} \frac{\partial \text{net}_{pk}}{\partial y_{pj}} = -\sum_k \delta_{pk} w_{kj} \quad (9)$$

Equations (8) and (9) are, respectively, valid for the output and hidden neurons and show how the analysis proceeds from output layer to proceeding layers. So quantities  $\delta_{pj}$  can be calculated in parallel for all output neurons  $j$  as

$$\delta_{pj} = (ty_{pj} - y_{pj})(1 - y_{pj})(1 + y_{pj}) \quad (10)$$

The following quantities  $\delta_{pj}$  for all hidden layers can be then written by using Eq. (6)

$$\delta_{pj} = (1 - y_{pj})(1 + y_{pj}) \sum_k \delta_{pk} w_{kj} \quad (11)$$

where  $j$  refers to a neuron in one of the hidden layers, and the summation is over all neurons  $k$ , which receive signals from neuron  $j$ . Substituting Eqs. (10) and (11) into Eqs. (4) and (5), steepest descent directions for current weights and biases are obtained. The weights  $w_{ji}$  and biases  $\theta_j$  are changed according to the following equations

$$\Delta w_{pj}(t) = \alpha \sum_p \delta_{pj} y_{pi} + \beta w_{pj}(t-1) \quad (12)$$

$$\Delta \theta_j(t) = \alpha \sum_p \delta_{pj} + \beta \theta_j(t-1) \quad (13)$$

where  $t$  indexes the number of times to train the neural model,  $\alpha$  is learning coefficient,  $\beta$  is momentum coefficient, which determines effect of past weights' changes on current direction of movement in the weight surface.

Training an MLP by BPM to compute RF EMFs involves presenting it sequentially with different input set (RF output power and measurement time) and corresponding target value (RF EMF). Errors between target and neural model outputs are back propagated through the network to adapt its weights using Eqs. (12) and (13). The training explained earlier is known as pattern-based training, which is faster than batch training where the weights are only modified once all the tuples in training set have been presented to the network.

A training epoch is completed after all tuples (sets) in the training set applied to the network. Training is stopped when RF EMF accuracy of the network is deemed satisfactory according to some criterion such as the root-mean-square (RMS) error between the target fields and neural model outputs for all the training set falling below a given threshold RMS error (0.005) or the maximum allowable number of iterations (12,000) is reached.

In this work, all features of ANNs (generalization, fast real-time application, ease of implementation, and providing approximate solution to the difficult problems) were adopted to estimate 3D screening of RF EMF distribution around TV transmitter antennas. Estimating results of RF EMFs at different output power and measurement time around TV broadcast transmitter has been presented. Visual software, which has 3D screening unit, based on ANN has been developed. So, the amounts of RF EMFs at different output power and measurement time, in and out of the measurement points, were estimated and visualized.

#### 4. RF FIELD DISTRIBUTION (FD) BASED ON ANNS AND GRIDDATA

To determine 3D screening of RF EMF distribution of TV transmitter, intelligent software was developed based on ANNs, which might estimate the values of RF EMFs at nonmeasured points using the data obtained from previous measurements. Software consists of four menus (design, training, test, and settings) which are as follows (see Fig. 4):

##### 4.1. Design Menu

Antennas and map of interested area were used to design the working environment. Objects (antenna and building, etc.) representing equipment were used to create design menu and then used to design the project (see Fig. 4). Objects were sensitive to change the place and the position. Mouse support was used to simplify the design stage. A single file construction was preferred to make the project control easily.

This menu was designed to create antenna and building symbols and to store map of area. Symbols created previously and map were stored under this menu in a file. Using design menu, it is always possible to create new symbols as well. If there is a stored project in the file, it can be read from file and monitored on the design frame at any time. Modifications can then be easily done on it. It should be emphasized that the design frame is very sensitive to the coordinates.

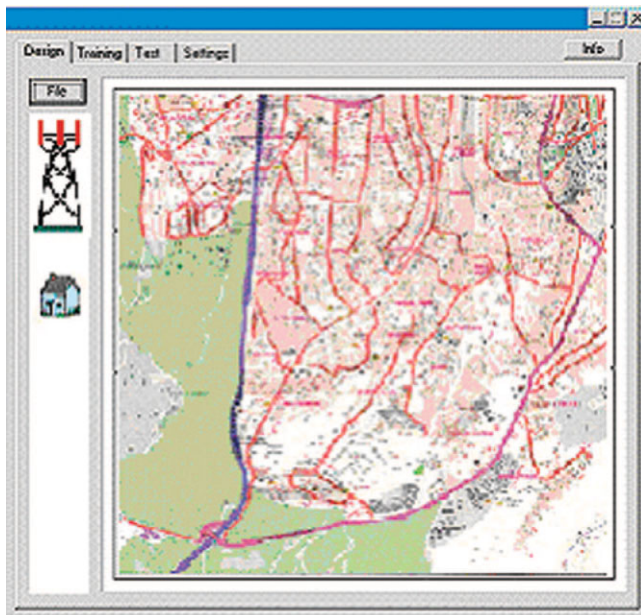


**Figure 4** Design frame for design menu. [Color figure can be viewed in the online issue, which is available at [www.interscience.wiley.com](http://www.interscience.wiley.com)]

It is possible to set the symbols (equipment, component) into their real own places on the allocation plan by clicking on the boxes of these components. When these components are being settled down, coordinates of them can be seen by opening properties window using right button of mouse. The component (only antenna and building in this study) is placed into requested point. If this component is not placed on the right area, coordinates and positions of them can be changed by using the right button of mouse. It is possible to copy same components many times on the allocated plan using the developed program. By this way, components on the project can be achieved easily. The program saves coordinate values for each component. It then enables the users to see, to compare, and to evaluate the field changing in 2 and 3 dimensions.

#### 4.2. Training Menu

To reduce training time, registers were used in programming. This menu includes the procedure of prediction using ANN algorithm that represents brain of developed software. Measurement values in allocation project of RF EMFs were used to train ANNs. If ANN was a closed box, output power of the transmitter and measurement time values taken from the system were accepted as inputs to ANNs. The output of ANN was total RF EMF measured from system input at 22 different points of near transmitter antenna. Total effective value of measured RF EMF is the absolute value of total vector of components on that point in space. While the numbers of training data sets composed of different measuring fields in different input conditions increase, obviously, training and learning capability of ANN will be improved. After saving data into the system for training, ANN starts to learn them by clicking the training button.

The program is sensitive to screen coordinates. Therefore, coordinates of settled measurement points can be observed on the screen. If a signed measurement value is positioned into a wrong place, it can be brought to the right coordinates on the project as dragging. When the mouse is put on any point on the project in the design menu, coordinates on this point can also be seen. Coordi-

nates of the measurement points signed here were saved for further processes to be used for graphic applications.

The data taken from measurement equipment through RS232 cable can be saved into a file in the system. But this part of the program was not tested. The working frame is suitable for saving the input data manually. These data can be then deleted when required.

In this study, ANNs were trained with the help of standard back propagation algorithm. Weights of ANNs were modified according to negative gradient of error measurement depending on Eqs. (12) and (13). Sigmoid function was chosen as a transfer function in three hidden layers of ANN model. The steps followed in the developed software are as follows: (1) allow the user to choose a component from the symbol menu and to put them on the design menu and continue with step (1) until the design is be completed; (2) take the measurement points and values on the designed transmitter area, register the values and continue with step (2) until all the points are considered; (3) send the measurement points and values to ANN model for training; (4) take input values (RF output power and measurement time) from the user; (5) send the values to the ANN model in test to produce the estimated results; (6) compose an estimated RF EMF distribution by sending produced estimated values to surface fitting model; and (7) monitor the values and surface to the user.

#### 4.3. Test Menu

Test menu consists of two parts: (i) field distribution occurred around the transmitter for an unknown input set is calculated; and (ii) visual evaluation and comparison of the obtained outputs are then achieved in graphical form. Test menu starts working after completing training of ANN. It calculates different field distribution for different inputs, which were not known or seen previously.

Mathematics libraries of C++ and Matlab were used for graphic designs in graphic option in test module. Basically, marking processes of "GridData" procedure, which is based on a Delaunay triangulation of the data that uses Qhull [18], were realized for surface fit. GridData enables multiline and multishape text viewing and editing in a floating or docked, resizable window and can export to text files, and sum or average the numeric data in columns.

Three dimensional charging [supplied visual facility as also using the colors on surface (Fig. 5a), three dimensional network output (Fig. 5b), and two dimensional approaches also added the factors of overview to platform and color in changing depicted (Fig. 5c)] were demonstrated. Furthermore, EMF value can be seen on any point as dragging mouse to a required location.

Outputs of ANNs were also represented in two-dimensional RF EMF distributions. Furthermore, field value can be seen at any point as dragging mouse to the required location. The name of axes can easily be written on graphic by marking corresponding boxes seen on graphic. Moreover, developed software automatically determines and shows maximum and minimum values of related RF EMFs.

#### 4.4. Settings Menu

In this menu, some parameters can be set to the related algorithm used for ANN training. Settings menu was used to set the parameters of ANN, which are number of neurons in hidden layer, upper limit of error rate on calculation, learning rate, and number of iteration. Other parameters for setting are EMFs limited to threaten value for human health and other electronic equipment.

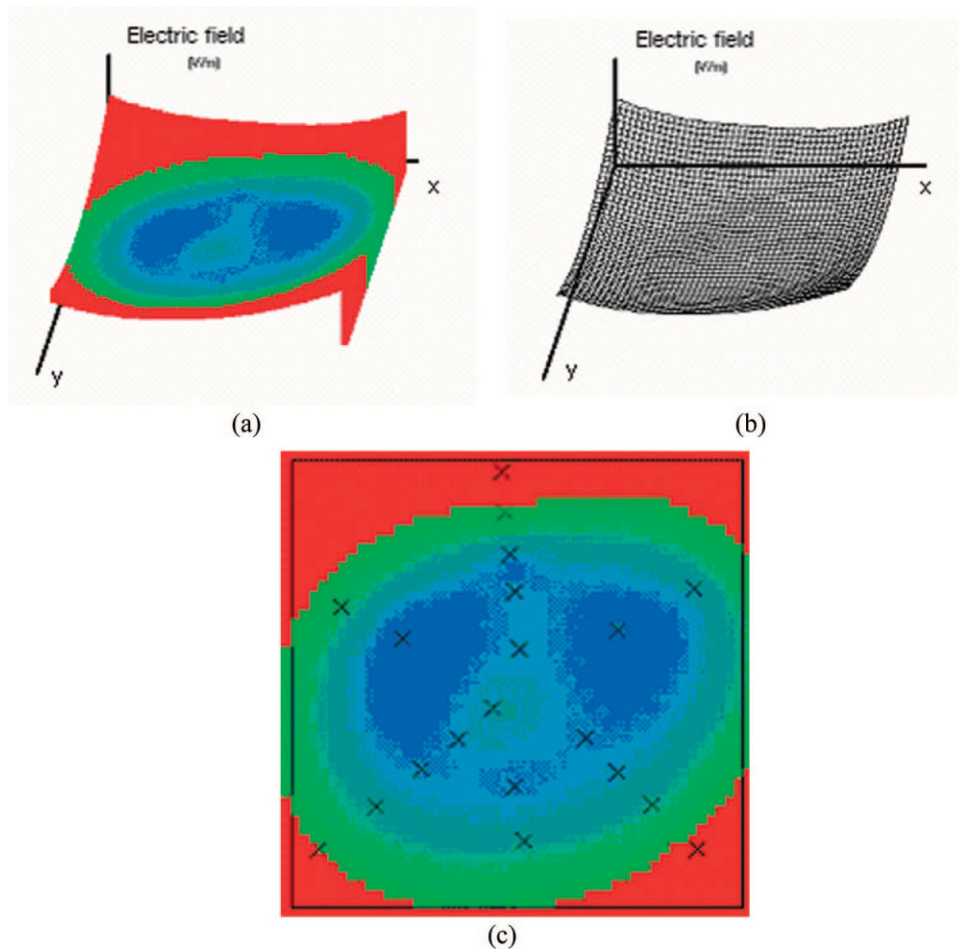


**Figure 5** Electric field distributions in 2D and 3D (a) 3D coloured, (b) 3D grid, (c) 2D colored. [Color figure can be viewed in the online issue, which is available at [www.interscience.wiley.com](http://www.interscience.wiley.com)]

#### 4.5. Estimation Results for Different RF Output Power

The developed ANN based program and the measuring meter provide closer look at variation of RF EMF density within some specified locations around transmitter and present direct comparison between measured and estimated RF EMFs at that defined locations around the transmitter. It can be observed that the simulation (estimation) agrees with measurements since overall distributions of fields are similar.

The inputs taken from 500 W, 750 W, and 1500 W operation condition were used to train ANN models. Outputs were also measured from the transmitters at 1.75 m high at 22 different points. ANN models having two inputs and 22 outputs were trained in three different operation conditions. RF EMFs measured near the transmitter and never used in training of ANNs were considered in test of the system. Inputs and outputs considered in test were taken under three different test conditions, which were not used in training. Test results belonged to the conditions 600 W, 850 W, and 1250 W and measured values at the same point are compared. Comparison of three different state are similar to each other, one comparison is presented in Figure 6 for 850 W output power. ANN parameters were as follows: 3 hidden layered network; learning rates, 0.3; and number of iteration, 12,000. Input and output values were normalized in between [0 and 1] intervals.

## 5. RESULTS

Measurements of RF EMFs at one output power around a TV transmitter were presented and also three set measurement belong-

ing to different output power and measurement time were implemented. It was found that all the measured RF EMFs levels were significantly lower than the ICNIRP 1998 Guidelines.

Visual software having 3D screening unit based on ANN and GridData has been developed. Amounts of RF EMFs at different operation conditions in and out of the measurement points around the transmitter were estimated with ANN and GridData models. This reduces determination cost and time of investigation of EMF distribution around the transmitter. The benefits of accurately predicting RF EMF distribution around TV transmitter are proper

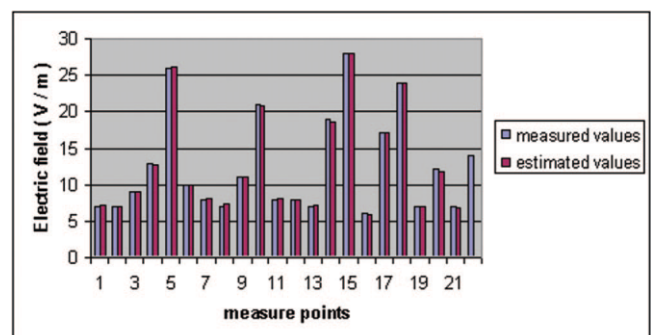


**Figure 6** Results for 850 W operation condition. [Color figure can be viewed in the online issue, which is available at [www.interscience.wiley.com](http://www.interscience.wiley.com)]

design of transmitter with the radiation issue in mind, risk estimation of exposure to RF EMF, and better understanding of the electric and magnetic properties of biological tissues. ANN based software in this study can estimate RF EMF distributions concerning all operating conditions, only making some measurements. So, researchers do not need many system data and calculation methods.

## 6. CONCLUSIONS

Results based on ANN model were found accurate and sufficient. This program enables users to estimate the distribution of RF EMF even out of the measurement points. The use of ANN allows users to analyze the system having less system data. 3D screening provides more visual environment to the researchers. EMFs measured at or around the transmitter centers can be compared with the standard values that how much they are in the limit values. EMF data can easily be taken into developed software so that the use of RS-232 is not necessary for this application. New adaptations to the software developed for the different design environments can be made. This study might also be adapted to similar studies on EMF distributions of base stations.

## REFERENCES

1. IEEE recommended practice for the measurement of potentially hazardous electromagnetic fields-RF and microwave, IEEE C95.3-1991.
2. A practical guide to the determination of human exposure to radiofrequency fields, NCRP Report no. 119, 1993.
3. Evaluating compliance with FCC guidelines for human exposure to radio frequency electromagnetic fields, FCC OET Bulletin 65, 1997.
4. ICNIPR Guidelines, Guidelines for limiting exposure time varying electric, magnetic and electromagnetic fields, Health Phys 74 (1998), 494–521.
5. A.S. Al-Ruwais, Measurements of RF radiation near MW and SW radio broadcast stations, IEEE Trans Broadcast 44 (1998), 470–477.
6. J.N. Sahalos, E.E. Vafiadis, T.S. Samaras, D.G. Babas, and S.S. Koukourlis, Em field measurements in the vicinity of an antenna park for radiation hazard purposes, IEEE Trans Broadcast 41 (1995), 130–136.
7. S. Özen, S. Helhel, and O.H. Colak, Electromagnetic field measurement of radio transmitters in urban area and exposure analysis, Microwave Opt Technol Lett 49 (2007), 1572–1578.
8. M. Kahski and L. Stasiński, Electromagnetic field estimation in the vicinity of panel antennasystem for FM and TV broadcasting, IEEE Trans Broadcasting 41 (1995), 136–143.
9. A. Faraone, R.Y.-S. Tay, K.H. Joyner, and Q. Balzano, Estimation of the average power density in the vicinity of cellular base-station collinear array antennas, IEEE Trans Vehicular Technol 49(2000), 984–997.
10. W.-T. Shay, R.-R. Lao, W. Liang, Practical measurement procedure for EM radiation from base stations in Taiwan, Asia-Pacific conference on environmental electromagnetics, CEEM' 2003, Nov. 47, 2003, Hangzhou, China.
11. R. Cicchetti and A. Faraone, Estimation of the peak power density in the vicinity of cellular and radio base station antennas, IEEE Trans Electromag Compat 46 (2004), 275–291.
12. E. Larcheveque, C. Dale, M.-F. Wong, and J. Wiart, Analysis of electric field averaging for in situ radiofrequency exposure assessment, IEEE Trans Vehicular Technol 54 (2005), 1245–1251.
13. W. Joseph, L. Verloock, and L. Martens, Reconstruction of the polarization ellipse of the EM field of telecommunication and broadcast antennas by a fast and low-cost measurement method, IEEE Trans Electromag Compat 48 (2006), 385–396.
14. A. Aren, C. Harston, and R. Pap, Handbook of neural computing applications, Academic Press, London, 1990, pp. 25–100.
15. S. Aykin, Neural networks: A comprehensive foundation, Macmillan College Publishing Company, New York, 1994, pp. 10–85.
16. D.T. Pham and S. Sagirolu, Training multilayered perceptrons for

pattern recognition: A comparative study of four training algorithms, Int J Mach Tools Manuf 41 (2001), 419–430.

17. D.E. Rumelhart and J.L. McClelland, Parallel distributed processing, 1986, p. 1.
18. Available at: <http://www.msri.org/info/computing/docs/qhull/qh-eg.htm#2d>.

© 2008 Wiley Periodicals, Inc.

## SLOT-LOADED SHORTED PATCH FOR DUAL-BAND OPERATION

Amit Kumar Singh and Manoj Kumar Meshram

Department of Electronics Engineering, Center of Advanced Study, Institute of Technology, Banaras Hindu University, Varanasi-221005; Corresponding author: manoj\_meshram@rediffmail.com

Received 21 August 2007

**ABSTRACT:** A dual-band slot-loaded shorted rectangular microstrip antenna is proposed and investigated both theoretically and experimentally. The dual-band characteristic of antenna is achieved by incorporating a shorting-pin on the left edge of the patch and thin slot. Numerical results for the input impedance, Return loss, and radiation patterns are presented and compared with the measured results. Good agreement is obtained between computed and measured results. Frequency tunability ranges from 1.39 to 1.44 GHz (about 50.0 MHz) for lower resonance and from 4.37 to 4.44 GHz (70.0 MHz) for upper resonance are observed. The frequency ratios of about 3.0 for the two operating frequencies are obtained. By loading the slot and shorting pin on the patch the antenna size is reduced up to 37%. © 2008 Wiley Periodicals, Inc. Microwave Opt Technol Lett 50: 1010–1017, 2008; Published online in Wiley InterScience (www.interscience.wiley.com). DOI 10.1002/mop.23300

**Key words:** dual-band microstrip antenna; quarter-wave patch; shorted patch; frequency tunable antenna; shorting-pin loaded patch antenna

## 1. INTRODUCTION

With the recent advancement in telecommunication, the need for small antennas with dual-band behavior has greatly increased. Electronic equipment has rapidly reduced in physical size due to the development of integrated circuit, but the antenna for communication equipment still remain large compared with the equipment itself. Especially in mobile communication, the demand for compact antenna is quite strong, therefore the need arose for antennas that are small in size and have a broad bandwidth. In spite of attractive features of microstrip antenna like low profile, light weight, low fabrication cost, and small size, there is requirement for compact, broadband antennas for communication system such as synthetic aperture radar and global positioning system, which specially requires dual or multifrequency operation. For these applications, a new motivation is given for research on innovative solution that overcomes the bandwidth limitation of patch antennas. For some applications in which increased bandwidth is needed for operating at separate sub-bands. A valid alternative to the broadening of total bandwidth is represented by dual frequency patch antennas. Dual frequency antennas exhibit a dual resonant behavior in a single radiating structure.

Recently, there have been extensive studies on size reduction technique for microstrip patch antennas [1–6]. Therefore, shorted microstrip antenna is widely used because the short circuit antenna can realize the same resonant frequency at about half the size of the standard microstrip antenna [7]. The shorted microstrip an-